A multiscale material model for metallic powder compaction during hot isostatic pressing

B. Elguezabal [a,b,*], J.M. Martínez-Esnaola [a,b], R. Soler [c], E. Paños [c], J. Alkorta [a,b]

[a] CEIT-Basque Research and Technology Alliance (BRTA), Manuel Lardizabal 15, 20018 Donostia / San Sebastián, Spain
[b] Universidad de Navarra, Tecnun, Manuel Lardizabal 13, 20018 Donostia / San Sebastián, Spain
[c] Industria de Turbo Propulsores S.A., ITP Aero, Parque Tecnológico, Edificio 300, 48170 Zamudio, Spain

HIGHLIGHTS

- Constitutive model for metallic powders has been extended with Eshelby's model.
- Pressure-dependent viscoplastic model has been extended with mesoscopic FEM data.
- Extended constitutive model has been validated with experimental data.
- Extended constitutive model provides higher accuracy in real industrial cases.

GRAPHICAL ABSTRACT
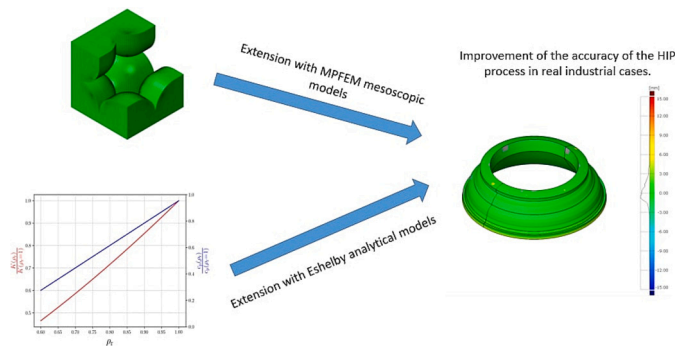
ABSTRACT

The prediction of the distortions during Near-Net-Shape Hot Isostatic Pressing (NNS-HIP) is an intrinsic multi-scale problem where the local interactions among particles determine the macroscopic distortions taking place during the sintering and densification of a component. In this work, a multiscale approach is proposed to solve this problem. In particular, a viscoplastic constitutive model capable of predicting macroscopic contractions during a HIP process with high accuracy has been developed, implemented and validated. The macroscopic model incorporates the mechanical behaviour predicted at the meso-scale by means of multiple-particle finite element models (MP-FEM) of an agglomerate of powder particles. The model is validated through the prediction of distortions during HIP of a full scale industrial case. It is concluded that adding the microscopic information of the HIP process to simulate the contractions at the macroscopic level results in a considerable improvement of the accuracy of the predictions.

1. Introduction

Nowadays, advanced powder metallurgy routes are widely used in the manufacturing of high quality and value components. These manufacturing processes were developed in the aeronautical sector, along with high-performance superalloys. These materials contain a

* Corresponding author at: CEIT-Basque Research and Technology Alliance (BRTA), Manuel Lardizabal 15, 20018 Donostia / San Sebastián, Spain.
  E-mail address: belguezabal@ceit.es (B. Elguezabal).

Table 1

Analytical expressions proposed for the evolution of the viscoplastic parameters.

Authors	A	B	η
Doraivelu [15]	$2 + \rho_r{}^2$	$\dfrac{(1 - \rho_r{}^2)}{3}$	$2\rho_r{}^2 - 1$
Lee and Kim [19]	$2 + \rho_r{}^2$	$\dfrac{(1 - \rho_r{}^2)}{3}$	$\left[\dfrac{\rho_r - \rho_{r0}}{1 - \rho_{r0}}\right]^2$
Shima & Oyane [14]	$\dfrac{3}{1 + \left(\frac{2.49}{3}\right)^2 (1 - \rho_r)^{1.028}}$	$\dfrac{\left(\frac{2.49}{3}\right)^2 (1 - \rho_r)^{1.028}}{1 + \left(\frac{2.49}{3}\right)^2 (1 - \rho_r)^{1.028}}$	$\dfrac{\rho_r{}^5}{1 + \left(\frac{2.49}{3}\right)^2 (1 - \rho_r)^{1.028}}$

higher amount of strengthening alloying elements, which lead to higher segregations and reductions in hot workability [1]. Among the different powder metallurgy processes, Hot Isostatic Pressing (HIP) has been used in industrial applications since the 70s [2]. In the HIP process, high temperature (about 70% of the melting point) and high pressure (up to 200 MPa) are simultaneously applied to encapsulated powder particles resulting in fully dense components and almost isotropic material properties [3].

The capability of HIP to produce near net-shape (NNS) components, which reduces the use of raw materials and minimizes the costs due to further machining processes, has been a major driving force for its commercial development. The accurate design of the tooling and the canister plays a key role in the NNS manufacturing via HIP. In this sense, the finite element method (FEM) stands out as the most promising tool for the design of the canisters used in HIP [4].

The main objective of this work is to predict the distortions during HIP processes on real components. The outline of the work is as follows. Mechanical tests have been carried out to characterize the viscoplastic behaviour of the fully dense Astroloy in the temperature range of the HIP processes. This is used, on the microscopic scale, to obtain the mechanical response of an agglomerate of metal powder particles by means of multiple-particle finite element (MP-FEM) simulations of simple cubic particle arrangements. A porous viscoplasticity model is then implemented in a CREEP subroutine in Abaqus® to simulate the HIP processing of an Astroloy powder encapsulated in an S355 steel canister. The model is calibrated using the multi-scale modelling approach together with the results of mechanical tests performed in partially dense and fully dense Astroloy compacts. Finally, comparison of the results, both using and not using the information generated at the microscopic level, indicates that the model with the input from the MPFEM analysis is about three times more accurate.

2. Review on porous material models

The accuracy of FEM modelling strongly depends on the adopted powder compaction constitutive model. In the FEM approximation, the powder is modelled as a continuum, whose behaviour is defined by a suitable material constitutive law in which powder compaction (inelastic deformation) occurs under hydrostatic pressure.

The constitutive models employed for the prediction of the powder behaviour during the compaction process are classified in two categories. The first type of models corresponds to frictional materials, which describe the behaviour of green metal powder [5]. The first model of this type was proposed in the 18th century by Coulomb [6]. However, it was not until the 1950s that Drucker and Prager [7] published their frictional model. Since the publication of this pioneering work, several authors have published their own extensions of the Drucker-Prager model [8–11].

The second type of constitutive models originates from the works published by Kuhn and Downey [12] and Green [13]. Several yield functions for porous materials can be found in the literature; some of them have been derived from experimental observations [12,14–16] and some others have been postulated based on micromechanical

considerations [13,17]. The main disadvantage of the empirical models is the lack of general information about the sintering process. For the case of the micromechanics-based models, the limitation of application to a certain porosity range is their main disadvantage. For example, the model proposed by Fleck et al. [17] is only suitable for high porosities. At porosities below about 0.25, the contacts start to interact, and the particles become less and less spherical in shape [18].

In general, both types of models include the dependence upon the hydrostatic stress (p) and the equivalent deviatoric stress (q), where p and q are calculated, respectively, as $\frac{\sigma_{kk}}{3}$ and $\sqrt{\frac{3}{2}s_{ij}s_{ij}}$, where $s_{ij} = \sigma_{ij} - \frac{1}{3}\sigma_{kk}\delta_{ij}$, σ_{ij} being the Cauchy stress tensor. The yield surfaces of all these constitutive models can be expressed by means of Eq. 1.

$$\phi = AJ_2 + B(I_1)^2 - \eta(\sigma_y)^2 = 0 \tag{1}$$

where I_1 is the first invariant of Cauchy stress tensor (σ_{ij}), J_2 is the second invariant of the deviatoric stress tensor (s_{ij}), σ_y is the yield stress of the dense material, and A, B, η are material parameters dependent on the relative density (ρ_r).

Table 1, generated from the work of Lee and Kim [19], summarizes the evolution of material parameters A, B and η with respect to the relative density (ρ_r) proposed by a number of authors in the bibliography.

Gurson [20] proposed a yield surface for porous materials derived from micro-mechanical considerations, analysing the behaviour of a spherical void in a material unit cell. This model is an extension of the classical von Mises plasticity model. The yield surface corresponding to Gurson's model is given by the following equation:

$$\phi = \frac{3J_2}{\sigma_y{}^2} + 2(1 - \rho_r)\cosh\left(\frac{I_1}{2\sqrt{3}\,\sigma_y}\right) - \left(1 + (1 - \rho_r)^2\right) = 0 \tag{2}$$

At high temperatures, metallic materials exhibit rate-dependent plasticity or creep [21]. For that reason, Abouaf et al. [2] and Svoboda et al. [22] developed viscoplastic constitutive models for porous metallic materials. In general, these viscoplastic constitutive models use the following expression for the equivalent stress (σ_{eq}):

$$\sigma_{eq}{}^2 = 3cJ_2 + fI_1{}^2 \tag{3}$$

where $c = c(\rho)$ and $f = f(\rho)$ are material parameters representing the contribution of the deviatoric and volumetric components of the stress tensor to the behaviour of the powder, respectively. The temperature and strain-rate dependence of these parameters is usually neglected in the literature.

Finally, the evolution of the inelastic strain (ε^{vp}) is typically defined as the derivative of a viscoplastic potential (Ω) with respect to the stress tensor (Eq. 4).

$$\dot{\boldsymbol{\varepsilon}}^{vp} = \frac{\partial \Omega}{\partial \boldsymbol{\sigma}} = \frac{\partial \Omega}{\partial \sigma_{eq}}\frac{\partial \sigma_{eq}}{\partial \boldsymbol{\sigma}} = \frac{\partial \Omega}{\partial \sigma_{eq}}\left(\frac{1}{\sigma_{eq}}\right)\left(\frac{3c}{2}\boldsymbol{s} + fI_1\mathbf{1}\right) \tag{4}$$

Eq. 4 is similar to the flow rule employed in conventional plasticity models [23], where $\partial \Omega / \partial \sigma_{eq}$ is the consistency parameter, which defines
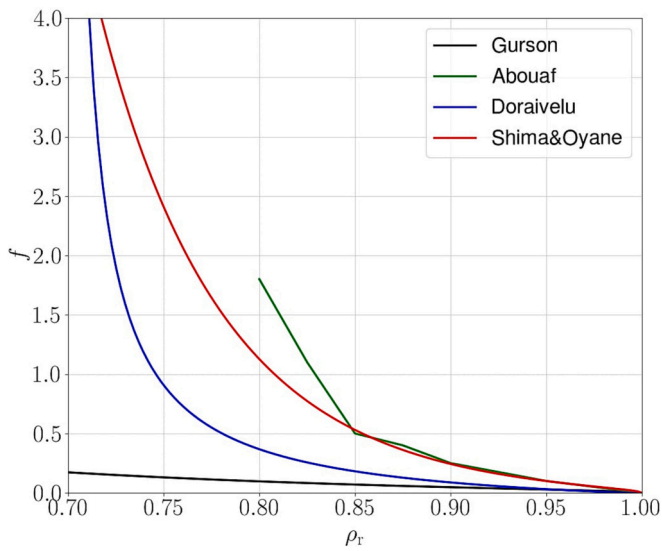
B. Elguezabal et al.

Powder Technology 425 (2023) 118599

Fig 1.. Graphical comparison of the hydrostatic parameter f of the works of Shima & Oyane [14], Doraivelu [15], Abouaf et al. [2] and Gurson[20].

the magnitude of the viscoplastic strain rate ($\dot{\varepsilon}^{\mathrm{vp}}$), and $\partial\sigma_{\mathrm{eq}}/\partial\boldsymbol{\sigma}$ determines its direction in the stress space [23]. Assuming associativity, a yield surface for Abouaf's viscoplastic model can be derived, which is an ellipse in the invariant plane $p - q$, as shown in Eq. 5. Taking the values of parameters c and f that Abouaf et al. determined in their work [2], a yield surface can be determined for a given viscoplastic strain rate.

$$\phi = c\left(\frac{q}{\sigma_{\mathrm{y}}}\right)^2 + 9f\left(\frac{p}{\sigma_{\mathrm{y}}}\right)^2 - 1 = 0 \tag{5}$$

Note that the first invariant of Cauchy stress tensor (I_1) and the second invariant of the deviatoric stress tensor (J_2) are proportional to, respectively, the hydrostatic stress (p) and the von Mises equivalent stress (q), so eq. 5 can be considered as a generalized form of yield surfaces for plasticity constitutive models of porous metals.

As can be seen in Fig. 1, a huge discrepancy is observed among the different studied models. This difference in the material constitutive models is due to the high sensitivity of the mechanical behaviour of the metallic powders to the shape, arrangement and distribution of particles and pores. This makes the calibration of a constitutive model for the prediction of shrinkage during a HIP process a very challenging task. In the present work, a multiscale simulation approach together with the experimental characterization carried out by Elguezabal et al. [24,25] will be considered to clarify the effect of the porosity on c and f (see eq. 3).

3. Material constitutive model and implementation

The densification of metallic powder compacts under high hydrostatic pressures and high temperatures is intrinsically a multi-scale problem where the macroscopic scale distortions are driven by the local micro-scale powder particle interactions. The model proposed in this paper is based on a multi-scale approach that stands on the continuum (macroscale) elastic-viscoplastic model framework considered in eq. (4).

In this model, the parameters $c = c(\rho, T, \dot{\varepsilon}^{\mathrm{vp}})$ and $f = f(\rho, T, \dot{\varepsilon}^{\mathrm{vp}})$ determine the viscoplastic flow under, respectively, deviatoric and hydrostatic stresses. These material parameters have been usually considered independent of the processing temperature and estimated through experimental tests [2,14–19] or excessively simple theoretical models [20]. In the present approach, they will be analyzed combining mesoscopic FEM simulations of representative volume elements (RVE) and experimental mechanical testing.

3.1. Macroscopic scale model

3.1.1. Elastic-viscoplastic model

To model the inelastic behaviour of Astroloy powder during the HIP process at high temperatures, the viscoplastic model developed by Abouaf et al. [2] has been employed. To begin with, an additive decomposition of the strain rate tensor ($\dot{\boldsymbol{\varepsilon}}$) into its elastic ($\dot{\boldsymbol{\varepsilon}}^{\mathrm{e}}$) and inelastic ($\dot{\boldsymbol{\varepsilon}}^{\mathrm{vp}}$) part is assumed:

$$\dot{\boldsymbol{\varepsilon}} = \dot{\boldsymbol{\varepsilon}}^{\mathrm{e}} + \dot{\boldsymbol{\varepsilon}}^{\mathrm{vp}} \tag{6}$$

Eq. 4 defines the evolution of the inelastic strain rate ($\dot{\boldsymbol{\varepsilon}}^{\mathrm{vp}}$). In this equation, the $\left(\frac{\partial\Omega}{\partial\sigma_{\mathrm{eq}}}\right)$ term defines the viscoplastic behaviour of the fully dense material. In this case, this term fits a creep law of the hyperbolic sine type, as shown in the following expression.

$$\frac{\partial\Omega}{\partial\sigma_{\mathrm{eq}}} = A_{\mathrm{c}}e^{-\frac{Q}{RT}}\left[sinh\left(\alpha\sigma_{\mathrm{eq}}\right)\right]^{n_{\mathrm{c}}} \tag{7}$$

where T is the current (absolute) temperature and A_{c}, n_{c}, α and Q/R define material parameters, which have been characterized in the present work.

Applying the law of conservation of mass, the expression that defines the evolution of the relative density as a function of the inelastic deformation is given by

$$\rho_r = \rho_{r0}e^{-\mathrm{tr}(\boldsymbol{\varepsilon}^{\mathrm{vp}})} \tag{8}$$

where ρ_{r0} defines the initial relative density.

In both the Svodoba et al. [22] and Abouaf et al. [2] models, the assumption is made that the parameters c and f only depend on the relative density. In the present work, the effect of temperature on these parameters has also been considered and included in the analysis.

For the elastic component of the powder model, an isotropic elastic behaviour dependent on temperature and relative density has been assumed. This can be written in the form

$$\boldsymbol{\sigma} = \lambda\mathrm{tr}(\boldsymbol{\varepsilon}^{\mathrm{e}})\mathbf{1} + 2\mu\boldsymbol{\varepsilon}^{\mathrm{e}} \tag{9}$$

where λ and μ are Lamé's coefficients, which can be defined as function of elastic modulus (E) and Poisson's coefficient (v) as follows:

$$\lambda = \frac{Ev}{(1+v)(1-2v)}$$

$$\mu = \frac{E}{2(1+v)} \tag{10}$$

The experimental characterization of these parameters as a function of temperature and relative density is time-consuming and expensive and it is not available in the literature. Therefore, approximate semi-analytical methods have been employed in this work for the prediction of average properties of multiphase materials.

3.1.2. Eshelby approach to determine physical properties of porous materials

Most models used to predict the average properties of a multiphase material are based on the work of Eshelby [26], who studied the behaviour of an elastic matrix with an ellipsoidal inclusion. Applying the theory developed by Eshelby, a differential equation (eq. 11) is obtained, which relates the change in the elastic properties of the compound for every increase in the volume fraction of the inclusion [25].

$$\frac{d\mathbb{C}_{\mathrm{c}}}{dv_{\mathrm{f}}} = \frac{1}{1-v_{\mathrm{f}}}(\mathbb{C}_{\mathrm{i}} - \mathbb{C}_{\mathrm{c}})\left[\mathbb{I} + \mathbb{S}\mathbb{C}_{\mathrm{c}}^{-1}(\mathbb{C}_{\mathrm{i}} - \mathbb{C}_{\mathrm{c}})\right]^{-1} \tag{11}$$

where $\mathbb{C}_{\mathrm{c}}$ and $\mathbb{C}_{\mathrm{i}}$ are the stiffness tensor of the composite and the inclusion (void), respectively, v_{f} is the volume fraction of voids. Finally, $\mathbb{S}$ is the Eshelby tensor, which is a function of the void geometry and the
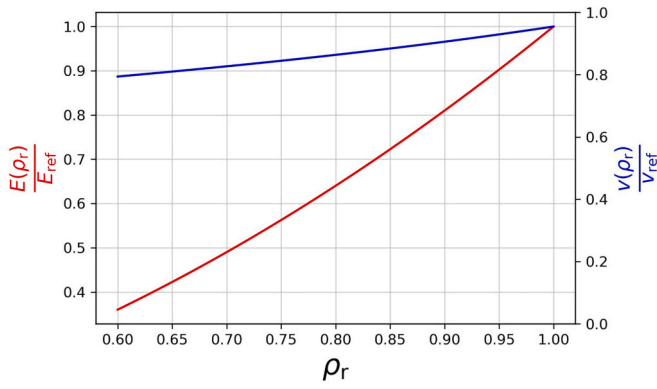
Fig. 2. Evolution of elastic modulus (red) and Poisson's modulus (blue) for different relative density levels.
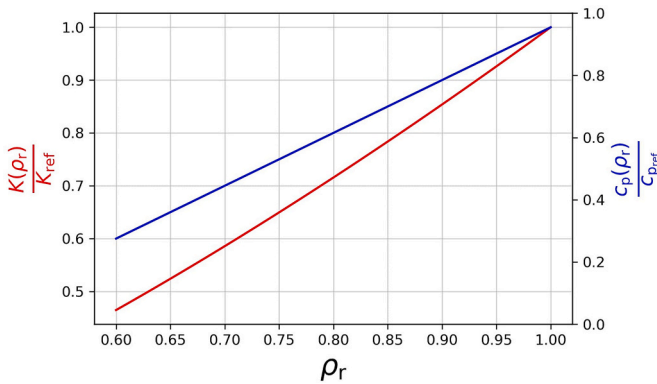

Fig. 3. Evolution of thermal conductivity (red) and specific heat capacity (blue) for different relative density levels.

matrix stiffness.

By solving the above differential equation numerically, the evolutions of the elastic modulus (E) and Poisson's coefficient (ν) of the composite material have been obtained (eqs. 12 and 13). Fig. 2 shows
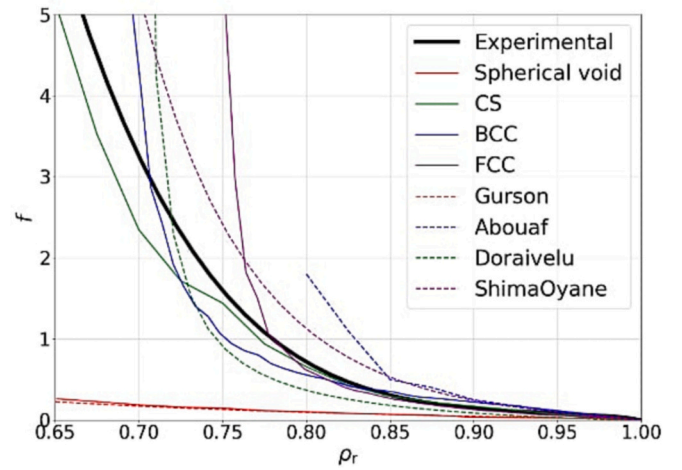

Fig. 5. Correlation obtained in [25] among experimental results, numerical results from FEM and bibliography results. Abbreviations for configurations: CS (Cubic Simple), BCC (Body Centered Cubic) and FCC (Face Centered Cubic).

Table 2
Cases considered for the study of the effect of temperature and strain rate on the hydrostatic (f) and deviatoric (c) parameters.

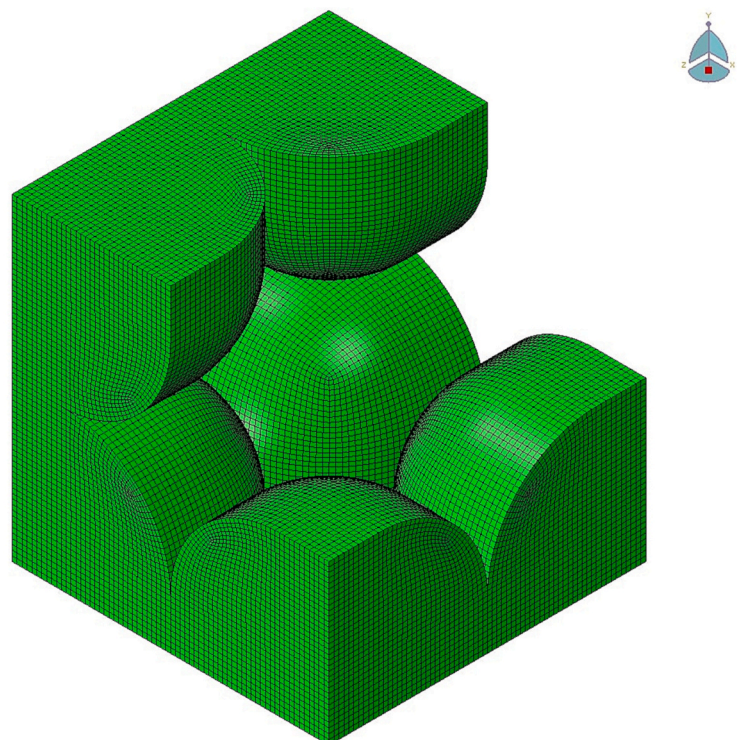| Case number	$T(°C)$	$\dot{\epsilon}^{vp}(s^{-1})$
1	1000	$6 \cdot 10^{-4}$
2	1000	$6 \cdot 10^{-5}$
3	1100	$6 \cdot 10^{-3}$
4	900	$6 \cdot 10^{-3}$

Fig. 4. Cut view of the mesoscopic finite element model used in [25] for the prediction of hydrostatic (f) and deviatoric (c) parameters.
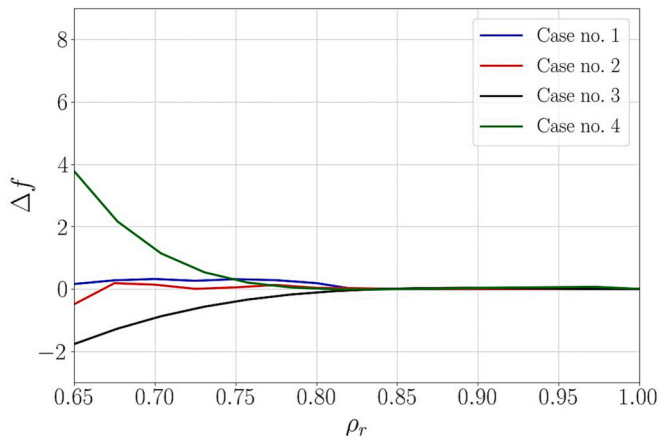
Fig. 6.. Difference of the hydrostatical parameter (f) obtained in cases from Table 2 with respect to the reference case.
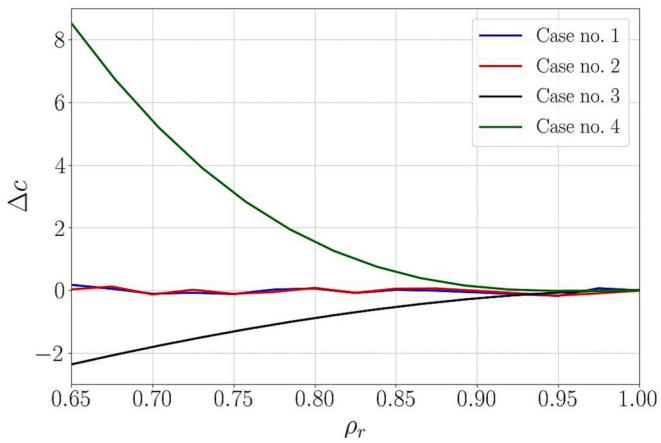

Fig. 7.. Difference of the deviatoric parameter (c) obtained in cases from Table 2 with respect to the reference case.
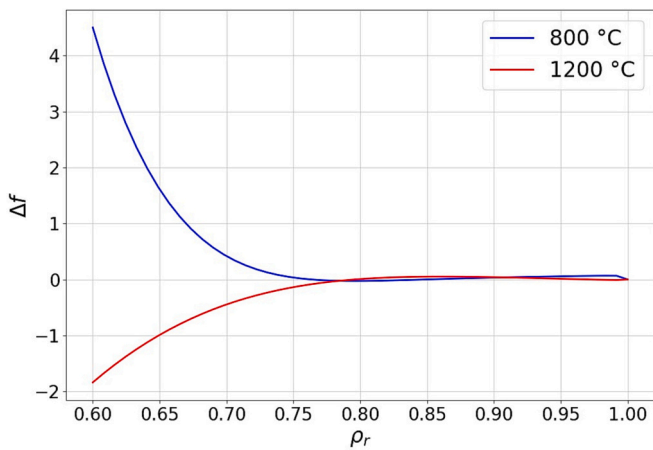

Fig. 8.. Difference of the evolution of hydrostatic parameter (f) for 800ºC and 1100ºC with respect to 1000 ºC.
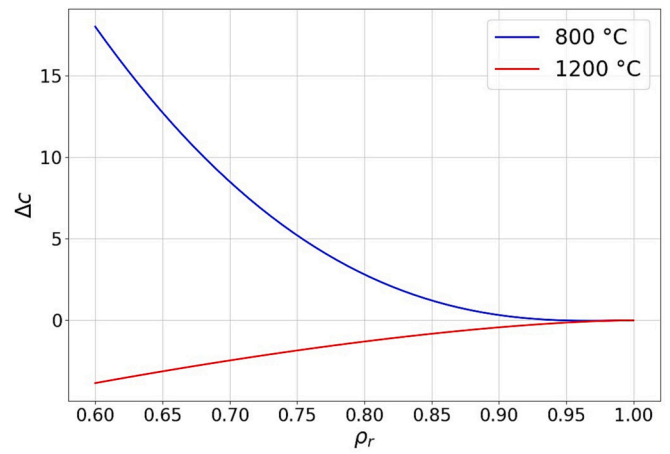

Fig. 9.. Difference of the evolution of deviatoric parameter (c) for 800ºC and 1100ºC with respect to 1000ºC.
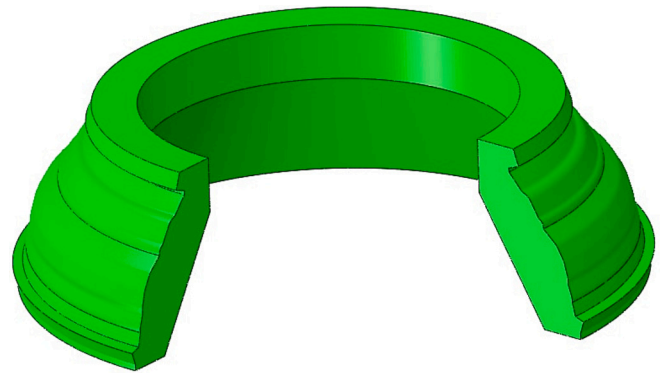

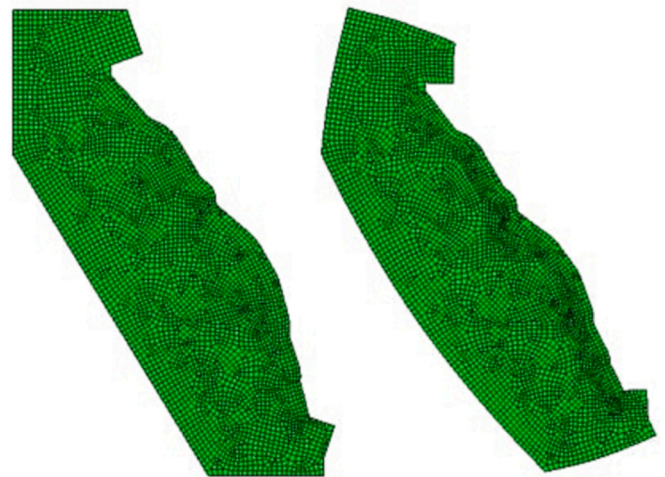**Fig. 10..** 3D geometry of the Astroloy cannister and powder assembly (Undeformed).

Fig. 11.. Mesh used to model the assembly of Fig. 8 in its undeformed (left) and deformed (right) configurations.

the evolution of these material parameters for different relative density levels.

$$\frac{E(\rho_r)}{E_{ref}} = \rho_r^2 \qquad (12)$$

$$\frac{\nu(\rho_r)}{\nu_{ref}} = 1 - \frac{0.122(1-\rho_r) - 0.09158(1-\rho_r)^2 + 0.04933(1-\rho_r)^3}{\nu_{ref}} \qquad (13)$$

Where E_{ref} and ν_{ref} define elastic modulus and Poisson's ratio at full dense state, which means a relative density (ρ_r) equal to one.
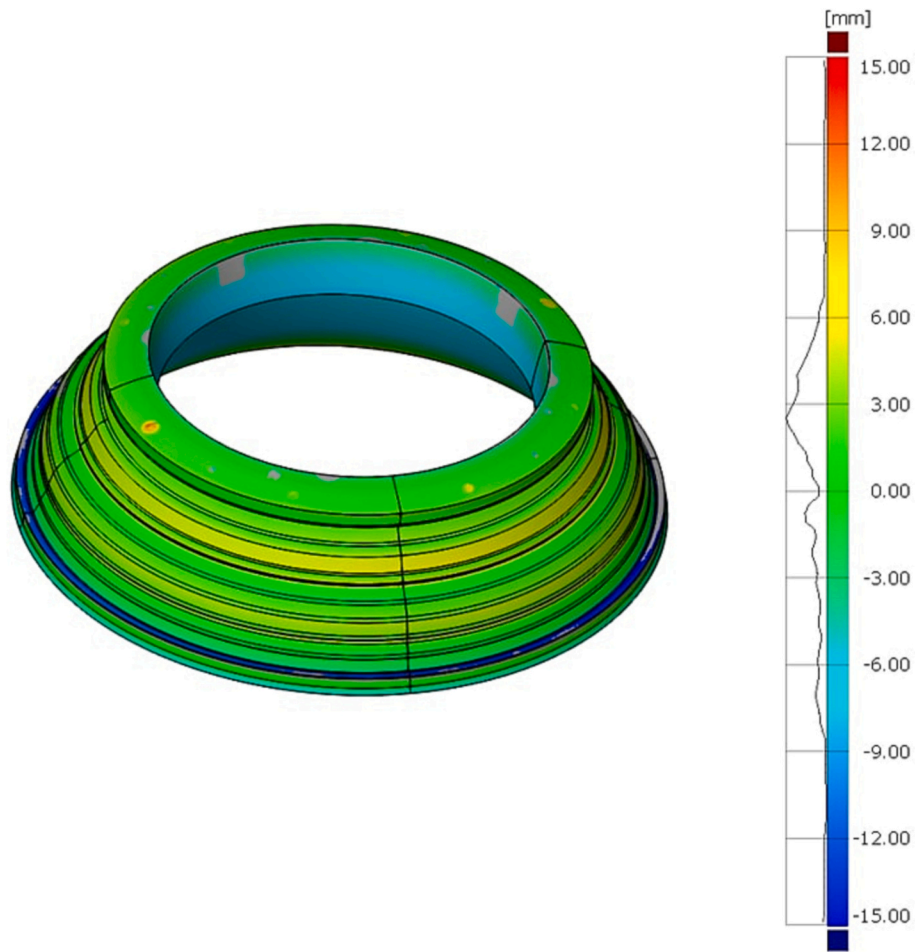
Fig. 12.. Deviations of the non-extended material model for a real industrial application.

The behaviour of a solid in a thermal problem, where the predominant mechanism of heat transfer is conduction, is determined by its thermal conductivity, specific heat capacity and density. By means of a modification of the previous approach, developed by Eshelby, the variation of the thermo-physical properties for different degrees of compaction of the powder metal material has been calculated. Indeed, eqs. 14 and 15 describe the conductivity (K) and the specific heat capacity (c_p) as a function of relative density. The evolution of the thermo-physical properties with respect to the relative density is shown in Fig. 3.

$$\frac{K(\rho_r)}{K_{ref}} = \rho_r^{1.5} \tag{14}$$

$$\frac{c_p(\rho_r)}{c_{p_{ref}}} = \rho_r \tag{15}$$

Regarding the material employed in the canister, a potential-type creep law has been employed to define the inelastic behaviour at high temperatures. More specifically, the creep law has been defined according to the following equation:

$$\dot{\boldsymbol{\varepsilon}}^{vp} = A_s q^{n_s} \tag{16}$$

where A_s and n_s are material properties defined over the desired temperature range.

3.2. Mesoscopic approach to powder compaction

The multiscale approach is a well-established procedure in the modelling of materials with specific microstructures, as it allows

drawing relevant conclusions on materials behaviour while considerably reducing the experimental work (or when no experimental procedure is available). The microstructure is usually modelled using a Representative Volume Element (RVE) with periodic boundary conditions (PBCs) so that infinitely large periodic systems can be simulated. Computational homogenization techniques are used to determine the material behaviour on the macroscale [27,28].

In a previous work, Elguezabal et al. [25] developed and validated a mesoscopic model that predicts the hydrostatic and deviatoric behaviour of an arrangement of metallic particles. In that work, the microscopic mechanical response of different simple particle arrangements, in particular, Cubic Simple (CS), Body-Centered Cubic (FCC), Face-Centered Cubic (FCC) structures were modelled. The relative size of voids determines the overall relative density of the system. In this work, it was demonstrated with experimental results that the cubic structure (CS) reliably reproduces the evolution of the hydrostatic parameter (f) for the analyzed batch of powder.

Regarding boundary conditions, those employed on RVE are generally defined such that the energy equivalence between the two scales, known as the Hill-Mandel condition, is preserved [23]. To satisfy this condition the following equation must be accomplished:

$$\overline{\boldsymbol{P}} : \dot{\overline{\boldsymbol{F}}} = \frac{1}{V_0} \int_{V_0} \boldsymbol{P} : \dot{\boldsymbol{F}} dV \tag{17}$$

where $\boldsymbol{P}$ is the first Piola-Kirchhoff stress tensor, $\boldsymbol{F}$ is the deformation gradient and V_0 is the volume of the RVE.

Several different types of boundary conditions satisfy the Hill-Mandel condition; in the present work the periodic displacement and
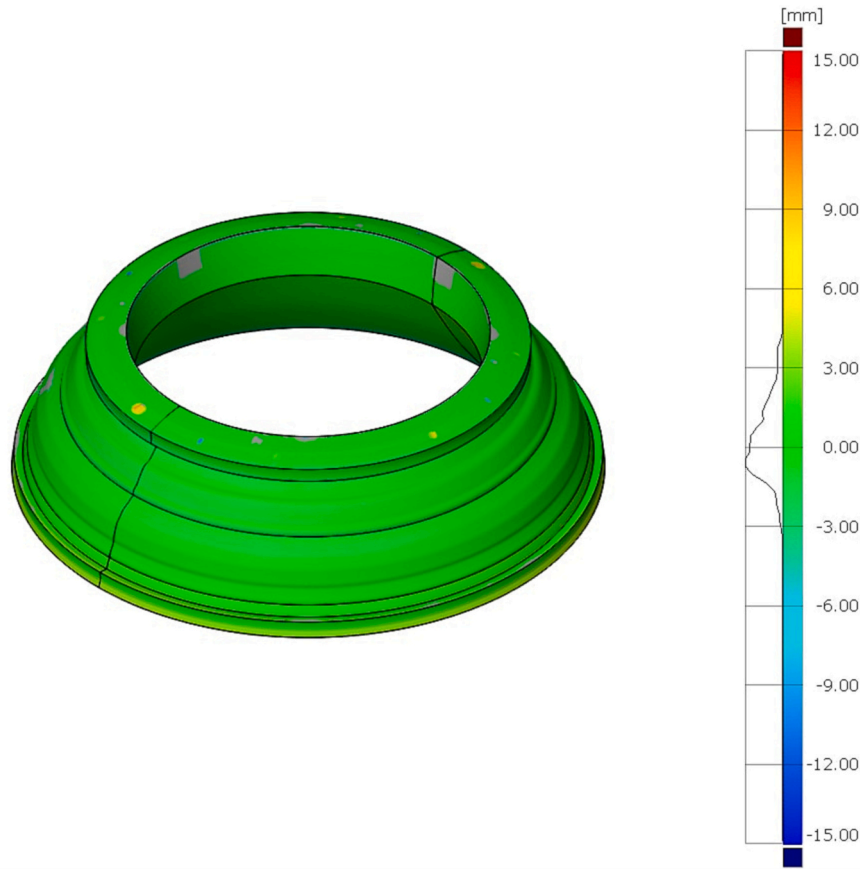
Fig. 13.. Deviations of the extended material model for a real industrial application.

antiperiodic traction boundary conditions have been employed. According to this periodic boundary condition, relative displacements at the boundaries between two contiguous unit cells must be connected properly to avoid inter-penetration or discontinuities [25]. In order to impose this relative displacement in the finite element calculations, three reference nodes (also known as dummy nodes) are included in the model.

The homogenization procedure based on the work of Loidolt [28] has been employed, where the macroscopic stress tensor is computed from the forces taken from the reference nodes and the current cross-sectional areas.

$$\overline{\sigma} = \begin{bmatrix} \dfrac{F_{xx}}{A_x} & \dfrac{F_{xy}}{A_x} & \dfrac{F_{xz}}{A_x} \\ \dfrac{F_{yx}}{A_y} & \dfrac{F_{yy}}{A_y} & \dfrac{F_{yz}}{A_y} \\ \dfrac{F_{zx}}{A_z} & \dfrac{F_{zy}}{A_z} & \dfrac{F_{zz}}{A_z} \end{bmatrix} \tag{18}$$

where, F_x, F_y and F_z represent the force vectors from the reference nodes and the second index determines their directional component, and A_x, A_y and A_z determine the cross sectional area of the YZ, XZ and XY planes, respectively, of the RVE cube.

By imposing different stress states, the values of the parameters f and c have been determined for different relative densities, temperatures and strain rates. Finally, the obtained results have been compared to experimental results in partially dense Astroloy powder compacts.

These results showed that, for a given temperature, a simple cubic (CS) arrangement of particles was optimum (in terms of the parameters c and f, see eq. 3) to describe the macroscopic behaviour of Astroloy compacts. Figs. 4 and 5 show the mesoscopic finite element model used

and its correlation with the experimental data for the hydrostatic case.

Both Abouaf et al. [2] and Svodoba [22] assumed that the hydrostatic and deviatoric parameters depend only on the relative density. In this work, we extend the mesoscopic approach detailed in [25] to account for the temperature and strain rate dependence of the parameters c and f (see eq. 3). To do that, we consider a simple cubic arrangement of particles (see Fig. 4). Its behaviour is simulated using multiple particle finite element models under different temperature and strain rate conditions.

The elastic-viscoplastic behaviour of these powder particles correspond exactly to a hyperbolic sine creep law that was fitted to experimental mechanical tests in a previous work [25]. As a reference, we will also consider the values of c_{ref} and f_{ref} obtained in [25] and validated experimentally with fully dense and partially dense samples obtained at $T = 1000°C$ and $\dot{\epsilon}^{vp} = 6·10^{-3}s^{-1}$.

From the current mesoscopic models, the deviations of c and f were calculated with respect to these reference values (f_{ref} and c_{ref}), i.e.:

$$f(\rho, T, \dot{\epsilon}^{vp}) = f_{ref} + \Delta f(\rho, T, \dot{\epsilon}^{vp}) \tag{19}$$

$$c(\rho, T, \dot{\epsilon}^{vp}) = c_{ref} + \Delta c(\rho, T, \dot{\epsilon}^{vp}) \tag{20}$$

Four different cases were studied in [25] with different packing densities, see Table 2. Cases 1 and 2 determined the strain rate dependence of c and f. Cases 3 and 4 determined the temperature dependence of c and f.

Concerning the effect of the strain rate, Figs. 6 and 7 show that it is negligible compared to the effect of temperature both for f and c.

In contrast, Figs. 6 and 7 show that the hydrostatic and deviatoric parameters are temperature sensitive, since the difference of these parameters for various temperatures is in the same order of magnitude as the absolute value of the parameters themselves (see, for instance,

Fig. 1). The effect of temperature seems to be more relevant in the case of *c* compared to *f* (where the deviations from the reference value are only apparent for relative densities below 0.85).

Once the influence of temperature on the hydrostatic parameter (*f*) and the deviatoric parameter (*c*) has been demonstrated, the mesoscopic FEM model has been used to determine the evolution of these parameters in the temperature range between 800°C and 1100°C.

Specifically, the evolution of the hydrostatic and deviatoric parameters has been characterized for the following temperatures: 800 °C, 900 °C, 1000 °C and 1100 °C. Figs. 8 and 9 show the difference of the hydrostatic and deviatoric parameters (Δ*f* and Δ*c*, respectively) for the highest and the lowest temperatures with respect to the evolution of these parameters for a temperature of 1000 °C, which was characterized in the work of Elguezabal et al. [25]. As can be seen in Figs. 8 and 9, at higher temperatures the value of the hydrostatic parameter (*f*) decreases for low relative density values. However, above relative density values of 0.80, the value of the hydrostatic parameter is shown to be independent of temperature.

In the case of the deviatoric parameter (*c*), the increase in temperature leads to a reduction in the value of this parameter. Nevertheless, this value is only shown to be independent of temperature for very high values of relative density, around 0.97.

3.3. Implementation in FEM

As indicated above, the main objective of this work is to predict the distortions during HIP processes on real components. For this reason, both the data extracted from the experimental campaign and the data extracted from the mesoscopic scale finite element analysis have been included in a user subroutine in order to incorporate the viscoplastic material model for porous materials in a commercial finite element software (Abaqus®).

This task has been carried out by means of three different subroutines implemented in Abaqus®. First, a CREEP subroutine was developed to define and implement a user-defined viscoplastic behaviour, which is explained in section 3.1.1. Secondly, a USDFLD subroutine was written to define a field variable that represents the evolution of the relative density from eq. 8. Finally, the SDVINI subroutine was required to define the initial values of the state variables, which by default were initialised with a value of 0.0. In this case, the initial relative density is initialised with a value close to the Tap density of the metal powder to be modelled. The hydrostatic (*f*) and deviatoric (*c*) parameters are stored in these state variables as well. The values of these parameters are calculated from the information obtained in the MPFEM model, which depends on the relative density and temperature, as shown in Figs. 8 and 9.

4. Validation of FEM model

For the validation of the constitutive description of the metallic powder and its numerical implementation, the non-extended and extended material models have been applied to the design of a casing used in aircraft engines, in particular, the turbine casing. Extended is the term used to designate the inclusion of the mesoscopic information mentioned in paragraph 3 in the material model. This housing was manufactured using the powder metallurgical HIP route as a demonstrator for the HUC project [29], which is part of the CleanSky initiative funded by the EU Commission. As the casing is a revolution part, axial symmetry has been employed to model the component to reduce the computational cost of the calculations. Therefore, the component of revolution has been modelled as a section cut in 2D. Fig. 8 shows the 3D geometry of the Astroloy cannister and powder assembly in its undeformed configuration, i.e., before the HIP process. Fig. 9 shows the mesh used to model this assembly in its undeformed (left) and deformed (right) configurations.

To model the HIP process, a hydrostatic pressure has been applied along the entire outer surface, which varies in time according to the HIP cycle employed. For the thermal simulations, heat conduction has been considered in the interior of the solid, and radiation and convection heat transfer mechanisms with the environment. To define these heat transfer mechanisms (convection and radiation) with the environment, a convection factor of 100 W/m^2·K and an emissivity of 0.4 have been defined for the external face, which is totally exposed, and an emissivity of 0.2 for the case of the internal face. Finally, a time-varying ambient temperature is imposed according to the HIP cycle used.

As for the initial relative density, this has been defined with a value of 0.64, which was calculated once the amount of powder that has been introduced into the canister was known.

The dimensions of the compacted component, whose maximum diameter is in the order of 1500 mm, were measured using 3D scanning techniques. The .stl file generated by the 3D scanner contains a point cloud, which has been processed and compared with data obtained in the FEM calculations.

4.1. Results for the non-extended model

In these simulations, the hydrostatic (*f*) and deviatoric (*c*) parameters (see eq. 3) of the Astroloy viscoplastic model are independent of temperature, and the elastic and thermophysic properties are not density-dependent. Fig. 10 shows the results obtained with this "non-extended model". In this case, as shown in the histogram in Fig. 10b, deviations are found in the range from −9 mm to +6 mm, although most of the deviation accumulates in the range of 3–6 mm. This range of deviation would be excessive for applications such as the Near-Net-Shape HIP.

4.2. Results for the extended material model

As can be seen in Fig. 11, the extended material model provides a higher accuracy, with a maximum deviation of 4.5 mm. This maximum deviation is located near the filling tubes. Neglecting these very localised details, which have not been included in the model, the histogram next to the colour bar in Fig. 10a shows that the accuracy of the model is within the range of ±2 mm. This is a very high accuracy for a part of 1500 mm in diameter. Moreover, in the central area where the Astroloy component is located, the deviation of the numerical model is in the range of 1 mm. As concluded, the accuracy of the extended model is higher than that of the non-extended material model, being the former applicable for Near-Net-Shape processes. (See Figs. 12 and 13.)

5. Conclusions

A multiscale modelling approach is developed to simulate the distortion taking place in the densification of a component during NNS-HIP (Near Net Shape Hot Isostatic Pressing). The model considered is able to reproduce the distortions with high accuracy (errors less than 0.2%). Furthermore, the model has been extended to incorporate the results from the mesoscopic simulations by including the effect of relative density. The extended model has been shown to be three times more accurate than the original model without the information from the mesoscopic model, see Figs. 10 and 11.

The obtained results indicate that the proposed constitutive model together with its numerical implementation in finite element calculations provide an accurate tool that will enable the design of the necessary tooling for the NNS-HIP without excessive computational cost.

The mesoscopic model used in the current approach, albeit considering a very simple arrangement of particles, is shown to be accurate enough to describe the effect of porosity, strain rate and temperature on the mechanical response of an aggregate of spherical powder particles during the densification process.

CRediT authorship contribution statement

B. Elguezabal: Conceptualization, Writing – original draft, Data

curation, Formal analysis. **J.M. Martínez-Esnaola:** Conceptualization, Writing – review & editing, Supervision, Validation. **R. Soler:** Writing – review & editing. **E. Paños:** Writing – review & editing. **J. Alkorta:** Conceptualization, Writing – review & editing, Supervision, Validation.

Declaration of Competing Interest

The authors declare that they have no known competing financial interests or personal relationships that could have appeared to influence the work reported in this paper.

Data availability

The data that has been used is confidential.

Acknowledgement

References

[1] D. Furren, J. Noel, Evaluation of P/M U720 for gas turbine engine disk application, TMS (1996) 705–711.

[2] M. Abouaf, J.L. Chenot, G. Raisson, P. Bauduin, Finite element simulation of hot isostatic pressing of metal powders, Int. J. Numer. Methods Eng. 25 (1988) 191–212.

[3] M.H. Bocanegra-Bernal, Reviex hot isostatic pressing (HIP) technology and its applications to metals and ceramics, J. Mater. Sci. 39 (2004) 6399–6420.

[4] A.M. Abdelhafeez, K.E.A. Essa, Influences of powder compaction constitutive models on the finite element simulation of hot isostatic pressing, Proc. CIRP 55 (2016) 188–193.

[5] K. Biswas, Comparison of various plasticity models for metal powder compaction processes, J. Mater. Process. Technol. 166 (2005) 107–115.

[6] C.A. Coulomb, Essai sur une Application des Regles des Maximis et Minimis a Quelquels Problemesde Statique Relatifs, a la Architecture, Mémoires de l'Académie Royale divers savants 7 (1776) 343–387.

[7] D.C. Drucker, W. Prager, Soil mechanics and plastic analysis for limit design, Q. Appl. Math. 10 (2) (1952) 157–165.

[8] A. Khoei, Z. Molaenia, S. Keshavarz, Modeling of hot isostatic pressing of metal powder with temperature–dependent cap plasticity model, Int. J. Mater. Form. 6 (2013) 363–376.

[9] H. Chtourou, Modeling of the metal powder compaction process using the cap model. Part II: Numerical implementation and practical applications, 2002.

[10] J. Almanstötter, A modified Drucker-Prager cap model for finite element simulation of doped tungsten powder compaction, Int. J. Refract. Met. Hard Mater. 50 (2015) 290–297.

[11] K.H. Roscoe, J.B. Burland, "On the generalized stress-strain behaviour of "wet" clay", Papers for conference held in Cambridge, University Press, Cambridge, 1968, pp. 535–609.

[12] H.A. Kuhn, C.L. Downey, Deformation characteristics and plasticity theory of sintered powder materials, Int. J. Powder Metall. 7 (1971) 15.

[13] R.J. Green, A plasticity theory for porous solids, Int. J. Mech. Sci. 14 (4) (1972) 215–224.

[14] S. Shima, M. Oyane, Plasticity theory for porous metals, Int. J. Mech. Sci. 18 (6) (1976) 285–291.

[15] S. Doraivelu, H. Gegel, J. Gunasekera, et al., A new yield function for compressible P\M materials, Int. J. Mech. Sci. 26 (9–10) (1984) 527–535.

[16] Y. Corapcioglu, T. Uz, Constitutive equations for plastic deformation of porous materials, Powder Technol. 21 (2) (1978) 269–274.

[17] N.A. Fleck, L.T. Kuhn, R.M. McMeeking, Yielding of metal powder bonded by isolated contacts, J. Mech. Phys. Solids 40 (5) (1992) 1139–1162.

[18] P. Redanz, Numerical modelling of the powder compaction, Eur. J. Mech. A/Solids Cup 8 (3) (1998) 399–413.

[19] D. Lee, H. Kim, Plastic yield behaviour of porous metals, Metal Powd. Rep. 35 (4) (1992) 275–279.

[20] A.L. Gurson, Continuum theory of ductile rupture by void nucleation and growth: part I- yield criteria and flow rules for porous ductile media, J. Eng. Mater. Technol. 99 (1977) 2–15.

[21] H.J. Frost, M.F. Ashby, Deformation Mechanism Maps, Pergamon Press, Oxford, 1982.

[22] A. Svodoba, H. Häggblad, L. Karlsson, Simulation of hot isostatic pressing of powder metal component with an internal core, Comput. Methods Appl. Mech. Eng. 148 (1997) 299–314.

[23] J.C. Simo, T.J.R. Hughes, Computational Inelasticity, Springer, New York, 1998.

[24] B. Elguezabal, Simulación del proceso de prensado isostático en caliente mediante modelización por elementos finitos, PhD thesis., TECNUN, School of Engineering (University of Navarra), May 2020.

[25] B. Elguezabal, J. Alkorta, J.M. Martínez-Esnaola, Study of Astroloy powder compaction at high temperature under hydrostatic load using finite elements, Powder Technol. 381 (2021) 92–100.

[26] J.D. Eshelby, The determination of the elastic field of an ellipsoidal inclusion, and related problems, Proc. Roy. Soc. A (1957) 241–376.

[27] D. Garoz, F.A. Gilabert, R.D.B. Sevenois, S.W.F. Spronk, W. Van Paepegem, Consistent application of periodic boundary conditions in implicit and explicit finite element simulations of damage in composites, Compos. Part B 168 (2019) 254–266.

[28] P. Loidolt, M.H. Ulz, J. Khinast, Modeling yield properties of compacted powder using a multi-particle finite element model with cohesive contacts, Powder Technol. 336 (2018) 426–440.

[29] CEIT BRTA. http://huc-cs2.eu/, 2018, October 1.